Hindawi
Mathematical Problems in Engineering
Volume 2019, Article ID 1534560, 10 pages
https://doi.org/10.1155/2019/1534560

Research Article

A Novel Method of Dynamic Force Identification and Its Application

Nengjian Wang,[1] Qinhui Liu ,[1] Chunping Ren ,[1] and Chunsheng Liu[2]

[1]*College of Mechanical and Electrical Engineering, Harbin Engineering University, Harbin 150001, China*
[2]*Heilongjiang University of Science and Technology, Harbin 150022, China*

Correspondence should be addressed to Qinhui Liu; liuqinhui@hrbeu.edu.cn

Received 19 September 2019; Accepted 4 November 2019; Published 14 December 2019

Academic Editor: Weimin Han

In this paper, an efficient mixed spectral conjugate gradient (EMSCG, for short) method is presented for solving unconstrained optimization problems. In this work, we construct a novel formula performed by using a conjugate gradient parameter which takes into account the advantages of Fletcher–Reeves (FR), Polak–Ribiere–Polyak (PRP), and a variant Polak-Ribiere-Polyak (VPRP), prove its stability and convergence, and apply it to the dynamic force identification of practical engineering structure. The analysis results show that the present method has higher efficiency, stronger robust convergence quality, and fewer iterations. In addition, the proposed method can provide more efficient and numerically stable approximation of the actual force, compared with the FR method, PRP method, and VPRP method. Therefore, we can make a clear conclusion that the proposed method in this paper can provide an effective optimization solution. Meanwhile, there is reason to believe that the proposed method can offer a reference for future research.

1. Introduction

It is of great significance to solve the engineering problem about the identification of the dynamic loads acting on the practical engineering structure with the improvement of engineering requirements and the progress of engineering technology [1–3]. Load identification is a kind of inverse problem, which is ill posed. At the same time, in many practical engineering problems, it is not easy to promptly obtain the dynamic loads in virtue of technical limitations [4, 5]. In general, we will tend to use indirect methods to restore the expected load on actual engineering structures.

As well as known, the regularization method can be used to solve the ill-posed problem procedure which can be translated into a kind of unconstrained optimization problems [6–10]; then, some optimization algorithms are used to solve it, such as conjugate gradient (CG) method, memory gradient (MG) method, and supermemory gradient (SMG) method [11–13]. It is generally known that the CG method does not achieve global convergence for common functions under inexact line searches [14], whereas the MG method needs to deal with the trust region subproblem [15]. Although the SMG method is superior to CG and MG methods, in some cases, it is also not globally convergent [16]. However, the spectral conjugate gradient (SCG) method does a lot of important works among various methods for solving unconstrained optimization problems [17]. The SCG method combines the spectral gradient and the conjugate gradient. The choice of spectral parameters is crucially important for the SCG method [18]. In this paper, we propose an efficient mixed spectral conjugate gradient (EMSCG) method, a novel formula performed by using a conjugate gradient parameter which takes into account the advantages of Fletcher–Reeves (FR) method [19], Polak–Ribiere–Polyak (PRP) method [20], and variant Polak–Ribiere–Polyak (VPRP) method [21] is constructed. The purpose of this paper is to find an effective method to deal with unconstrained optimization problems. In this way, an unconstrained optimization problem can be represented as [22]

$$\min\left\{f(x) \mid x \in \Re^n\right\}, \tag{1}$$

where the nonlinear function $f(x)$: $\Re^n \longrightarrow \Re$ is a continuously differentiable function whose gradient is denoted by $g(x)$: $\Re^n \longrightarrow \Re$.

Furthermore, a sequence $\{x_k\}$ can be obtained in an algorithm for solving (1) and has the following forms [23–25]:

$$x_{k+1} = x_k + \alpha_k d_k, \tag{2}$$

where d_k is a search direction and α_k is the step size which is achieved by the one-dimensional search method. Usually, the exact line search is described as follows [26]:

$$f(x_k + \alpha_k d_k) = \min_{\alpha \geq 0} f(x_k + \alpha d_k). \tag{3}$$

It is well known that there are different ways to determine d_k. In the conjugate gradient (CG) method, d_k can be expressed by [27]

$$d_k = \begin{cases} -g_0, & k = 0, \\ -g_k + \beta_k d_{k-1}, & k \geq 1, \end{cases} \tag{4}$$

where β_k denotes a scalar parameter characterizing the conjugate gradient method. The best-known expressions of β_k are Hestenes–Stiefel (HS) [28], Fletcher–Reeves (FR) [19], Polak–Ribiere–Polyak (PRP) [20], and Dai–Yuan (DY) [29] formulas, which are defined by

$$\begin{aligned} \beta_k^{\mathrm{HS}} &= \frac{g_k^T y_{k-1}}{d_{k-1}^T y_{k-1}}, \\ \beta_k^{\mathrm{FR}} &= \frac{\|g_k\|^2}{\|g_{k-1}\|^2}, \\ \beta_k^{\mathrm{PRP}} &= \frac{g_k^T y_{k-1}}{\|g_{k-1}\|^2}, \\ \beta_k^{\mathrm{DY}} &= \frac{\|g_k\|^2}{d_{k-1}^T y_{k-1}}, \end{aligned} \tag{5}$$

respectively, where $\|\cdot\|$ denotes the Euclidean norm and $y_k = g_{k+1} - g_k$. At the same time, (5) corresponds to four different conjugate gradient methods, and different methods have a lot of deformations. For example, in [20], a variant of PRP is given; β_k is expressed as

$$\beta_k^{\mathrm{VPRP}} = \frac{\|g_k\|^2 - \left(\|g_k\| / \|g_{k-1}\|\right) g_k^T g_{k-1}}{\|g_{k-1}\|^2}. \tag{6}$$

The VPRP method inherits some excellent properties of the PRP method, such as good numerical performance. Liu and Li [30] proved that the VPRP method has global convergence and descending property under strong Wolfe line search.

In recent years, some scholars developed a new method, spectral conjugate gradient (SCG) method, for solving (1). In [31], the spectral gradient method for large-scale unconstrained optimization was introduced, which combined a nonmonotone line search strategy that guarantees global convergence with the Barzilai and Borwein method. Utilizing spectral gradient and conjugate gradient ideas, Chen and Jiang [32] proposed a spectral conjugate gradient method. In these algorithms, the search direction has the following form:

$$d_k = \begin{cases} -g_k, & k = 1, \\ -\theta_k g_k + \beta_k d_{k-1}, & k \geq 2. \end{cases} \tag{7}$$

However, the search direction of the spectral conjugate gradient method proposed by Birgin and Martinez does not satisfy the descent property, and of course, it does not have global convergence. In order to obtain global convergence, Wang et al. [19, 33] constructed the FR-type spectral conjugate gradient method; spectral parameters θ_k and β_k are expressed as

$$\begin{aligned} \theta_k &= \frac{d_{k-1}^T y_{k-1}}{\|g_{k-1}\|^2}, \\ \beta_k &= \beta_k^{\mathrm{FR}}. \end{aligned} \tag{8}$$

An important feature of this method is to satisfy the sufficient descent condition:

$$d_k^T g_k \leq -t\|g_k\|^2, \tag{9}$$

where $t > 0$ is a constant.

The CD-type spectral conjugate gradient method is proposed in [34]. Reference [35] provided a HS-type spectral conjugate gradient method. A spectral conjugate gradient method for the PRP type is introduced in [36]. All the above methods meet the sufficient conditions of decline (3).

Based on the above literature, an efficient mixed spectral conjugate gradient method with sufficient descent is proposed, which was abbreviated as the EMSCG method, and parameters θ_k and β_k are expressed as

$$\begin{aligned} \beta_k^{\mathrm{EMSCG}} &= \frac{\|g_k\|^2 - \max\left\{0, \left(\|g_k\| / \|g_{k-1}\|\right) g_k^T g_{k-1}, g_k^T g_{k-1}\right\}}{\|g_{k-1}\|^2}, \\ \theta_k &= c + \beta^{\mathrm{EMSCG}} \frac{g_k^T d_{k-1}}{\|g_k\|^2}, \end{aligned} \tag{10}$$

where c is a parameter and $c > 0$.

As we can see from the algorithm framework above, the EMSCG method is similar to other spectral conjugate gradient algorithms. However, we choose two different spectral parameters β_k^{EMSCG} and θ_k which is the main difference between the EMSCG method and the others.

The present paper is organized as follows. In Section 2, the properties of an efficient mixed spectral conjugate gradient method are introduced. The global convergence is proved in Section 3, while the analysis results compared with the FR method, PRP method, and VPRP method, which are given in Section 4. In the last section, we draw some

conclusions about an efficient mixed spectral conjugate gradient method.

2. Properties of an Efficient Mixed Spectral Conjugate (EMSCG) Gradient Method

The following is a detailed description of an efficient mixed spectral conjugate gradient (EMSCG) method.

First of all, let us state a question, the constructed d_k is a search direction. The following theorems and proofs are obtained.

Theorem 1. *Suppose that d_k and g_k are generated by using Algorithm 1, and the sufficient descent condition holds. Then,*

$$g_k^T d_k < 0, \tag{11}$$

for all $k \geq 1$.

Proof. By Algorithm 1, we have

$$\begin{aligned} g_k^T d_k &= g_k^T\left(-g_k\theta_k + \beta_k^{\mathrm{EMSCG}} d_{k-1}\right) \\ &= -\theta_k\|g_k\|^2 + \beta_k^{\mathrm{EMSCG}} g_k^T d_{k-1} \\ &= -\left(c + \beta_k^{\mathrm{EMSCG}}\frac{g_k^T d_{k-1}}{\|g_k\|^2}\right)\|g_k\|^2 + \beta_k^{\mathrm{EMSCG}} g_k^T d_{k-1} \\ &= -c\|g_k\|^2 < 0. \end{aligned} \tag{12}$$

Hence, (11) is proved. □

Theorem 2. *Parameter β_k^{EMSCG} satisfies*

$$0 \leq \beta_k^{\mathrm{EMSCG}} \leq \frac{\|g_k\|^2}{\|g_{k-1}\|^2}, \tag{13}$$

for all $k \geq 1$.

Proof. We know that this is the mixture of the three methods according to formula (10), and now it is explained in three cases.

(i) When $g_k^T g_{k-1} \leq 0$, we have

$$\beta_k^{\mathrm{EMSCG}} = \frac{\|g_k\|^2}{\|g_{k-1}\|^2} = \beta_k^{\mathrm{FR}}. \tag{14}$$

(ii) When $g_k^T g_{k-1} > 0$ and $(\|g_k\|/\|g_{k-1}\|) \leq 1$, we have

$$\beta_k^{\mathrm{EMSCG}} = \frac{\|g_k\|^2 - g_k^T g_{k-1}}{\|g_{k-1}\|^2} = \beta_k^{\mathrm{PRP}}. \tag{15}$$

(iii) When $g_k^T g_{k-1} > 0$ and $(\|g_k\|/\|g_{k-1}\|) > 1$, we have

$$\beta_k^{\mathrm{EMSCG}} = \frac{\|g_k\|^2 - \left(\|g_k\|/\|g_{k-1}\|\right) g_k^T g_{k-1}}{\|g_{k-1}\|^2} = \beta_k^{\mathrm{VPRP}}. \tag{16}$$

The proof is effectively completed. In addition, from the selection of spectral coefficient of Algorithm 1, we can select the different parameters c to optimize the numerical effect of Algorithm 1. □

3. Convergent Analysis of the Proposed Method

In order to study the convergence of the algorithm, some basic assumptions are given as follows:

Assumption A

(P1) The objective function is bounded by the following level:

$$L = \left\{x \in \Re^n \mid f(x) \leq f(x_0)\right\}. \tag{17}$$

(P2) The gradient g is Lipschitz continuous; that is, there exists a constant $L > 0$ such that, for any $x, y \in U$, we obtain

$$\|g(x) - g(y)\| \leq L\|x - y\|. \tag{18}$$

Lemma 1. *Suppose that the function f has the properties (P1) and (P2). d_k is a descent direction and α_k is obtained by (3); then,*

$$\sum_{k=1}^{\infty}\frac{\left(g_k^T d_k\right)^2}{\|d_k\|^2} < +\infty. \tag{19}$$

In [14, 37, 38], Dai and Yuan stated that (19) had been essentially proved by Zoutendijk and Wolfe.

Lemma 2. *Suppose that assumption A holds, sequences $\{g_k\}$ are generated by Algorithm 1; then,*

$$\lim_{k\longrightarrow\infty}\inf\|g_k\| = 0. \tag{20}$$

Proof. Suppose that (19) is not established, there is a constant $\gamma > 0$; for all $k \geq 1$, we have $\|g_k\| \geq \gamma$.

According to formula (7), we get

$$d_k + \theta_k g_k = \beta_k^{\mathrm{EMSCG}} d_{k-1}. \tag{21}$$

Then,

$$\left(d_k + \theta_k g_k\right)^T\left(d_k + \theta_k g_k\right) = \left(\beta_k^{\mathrm{EMSCG}}\right)^2\|d_{k-1}\|^2. \tag{22}$$

Exploiting (22), we have

$$\|d_k\|^2 + 2\theta_k d_k^T g_k + \theta_k^2\|g_k\|^2 = \left(\beta_k^{\mathrm{EMSCG}}\right)^2\|d_{k-1}\|^2. \tag{23}$$

Step 1. Choose x_1 and ε, and then calculate g_1. If $\|g_1\| \le \varepsilon$, then terminate; else go to the next step.
Step 2. d_k is computed based on (7).
Step 3. α_k is computed based on (3).
Step 4. Set $x_{k+1} = x_k + a_k d_k$.
Step 5. Set $k = k + 1$, and go to the step 2.

Algorithm 1

Then,

$$\|d_k\|^2 = -2\theta_k d_k^T g_k - \theta_k^2 \|g_k\|^2 + \left(\beta_k^{\mathrm{EMSCG}}\right)^2 \|d_{k-1}\|^2. \quad (24)$$

Combining (24) and Theorem 1, we have

$$\|d_k\|^2 = -2c\theta_k \|g_k\|^2 - \theta_k^2 \|g_k\|^2 + \left(\beta_k^{\mathrm{EMSCG}}\right)^2 \|d_{k-1}\|^2. \quad (25)$$

Dividing both sides by $(g_k^T d_k)^2$, we have

$$\begin{aligned} \frac{\|d_k\|^2}{\left(g_k^T d_k\right)^2} &= \frac{\|d_k\|^2}{c^2 \|g_k\|^4} \\ &= \frac{2\theta_k}{c\|g_k\|^2} - \frac{\theta_k^2}{c^2\|g_k\|^2} + \frac{\left(\beta_k^{\mathrm{EMSCG}}\right)^2}{c^2\|g_k\|^4}\|d_{k-1}\|^2. \end{aligned} \quad (26)$$

Then, we have

$$\begin{aligned} \frac{\|d_k\|^2}{\left(g_k^T d_k\right)^2} &\le \left(\frac{\|g_k\|^2}{\|g_{k-1}\|^2}\right)^2 \frac{\|d_{k-1}\|^2}{c^2\|g_k\|^4} - \frac{(\theta_k - c)^2}{c^2\|g_k\|^2} \\ &= \frac{\|d_{k-1}\|^2}{c^2\|g_{k-1}\|^4} + \frac{1}{\|g_k\|^2} - \frac{(\theta_k - c)^2}{c^2\|g_k\|^2} \\ &\le \frac{\|d_{k-1}\|^2}{c^2\|g_{k-1}\|^4} + \frac{1}{\|g_k\|^2} \\ &\le \sum_{i=1}^{k} \frac{1}{\|g_k\|^2} + \frac{1}{c^2\|g_1\|^2} \\ &\le \frac{k}{\gamma^2} + l\left(l = \frac{1}{c^2\|g_1\|^2}\right). \end{aligned} \quad (27)$$

Hence, we can obtain

$$\sum \frac{\left(g_k^T d_k\right)^2}{\|d_k\|^2} \ge \gamma^2 \sum \frac{1}{k + \gamma^2 L} \longrightarrow +\infty. \quad (28)$$

From the above discussion, we can see that it is in contradiction with Lemma 1. Therefore, the conclusion is established. □

4. An Example of Engineering Application

In this section, the present method is applied to an engineering example of the identification problem of dynamic force generated between conical pick and coal-seam structure.

4.1. Establishment of the Dynamic Force Model. An abridged general view of dynamic force between pick and coal-seam structure is plotted in Figure 1. For a deterministic multi-degrees-of-freedom structures, we can use a unified dynamic equation to represent it, which can be expressed by the following form [39]:

$$[\mathbf{M}]\{\mathbf{y}''(t)\} + [\mathbf{C}]\{\mathbf{y}'(t)\} + [\mathbf{K}]\{\mathbf{y}(t)\} = \{\mathbf{F}(x, y, z, t)\}, \quad (29)$$

where $\mathbf{M}$, $\mathbf{C}$, and $\mathbf{K}$ denote the mass matrix, damping matrix, and stiffness matrix, respectively; $\mathbf{F}(x, y, z, t)$ denotes the dynamic force column vector in different directions; $\mathbf{y}(t)$, $\mathbf{y}'(t)$, and $\mathbf{y}''(t)$ denote displacement response vector, velocity response vector, and acceleration response vector, respectively.

The displacement of the structure can be described as

$$\mathbf{y}(t) = \sum_{i=1}^{n} \boldsymbol{\varphi}_i q_i(t) = \boldsymbol{\Phi}\mathbf{Q}, \quad (30)$$

where $\boldsymbol{\Phi}$ denotes the matrix of mode and $\boldsymbol{\Phi} = [\boldsymbol{\varphi}_1, \boldsymbol{\varphi}_2, \Lambda, \boldsymbol{\varphi}_n]$ and $\mathbf{Q}$ denotes the displacement vector and time function in the generalized coordinates, $\mathbf{Q} = [q_1, q_2, \Lambda q_n]^T$.

Combined with equations (29) and (30), the dynamic equations represented by the physical coordinates are transformed into the modal coordinate system, and the n decoupled modal equations are described as

$$q_i'' + 2\xi_i\omega_i q_i' + \omega_i^2 q_i = \frac{\mathbf{F}_i(t)}{\mathbf{M}_i}, \quad (31)$$

where ξ_i denotes the i-order modal damping ratio and $\mathbf{M}_i$ and $\mathbf{F}_i(t)$ denote the generalized mass and the generalized force, respectively, and $\mathbf{M}_i = \boldsymbol{\varphi}_i^T \mathbf{M} \boldsymbol{\varphi}_i$, $\mathbf{F}_i(t) = \boldsymbol{\varphi}_i^T \mathbf{F}(t)$.

$\mathbf{x}_0'$ and $\mathbf{x}_0$ denotes the initial velocity and initial displacement of the system, respectively. Hence, the q_i in equation (30) is expressed as follows:

$$q_i(t) = q_{1i}(t) + q_{2i}(t). \quad (32)$$

$q_{1i}(t)$ is obtained by the homogeneous equation of equation (29), which is described as follows:

$$q_{1i}(t) = e^{-\xi_i\omega_i t}\left(q_{i0}(t)\cos\left(\omega_{\mathrm{id}}t\right) + \frac{q_{i0}' + \xi_i\omega_i q_{i0}(t)}{\omega_{\mathrm{id}}}\sin\left(\omega_{\mathrm{id}}t\right)\right). \quad (33)$$

Here, q_{i0} and q_{i0}' are the corresponding values in modal coordinates; it is described as follows:

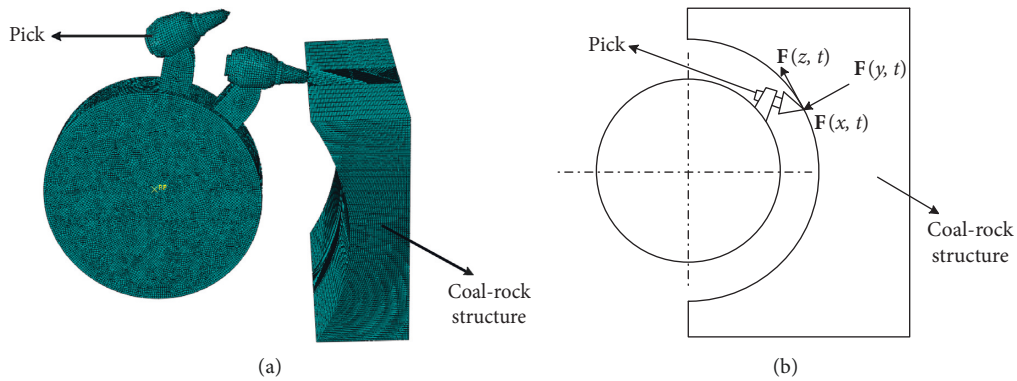

Figure 1: Schematic of dynamic forces between pick and coal-seam. (a) Pick and coal-seam structure. (b) Dynamic forces.

$$q_{i0} = \frac{\boldsymbol{\varphi}_i^T \mathbf{M} x_0}{M_i}. \tag{34}$$

Here, q_{2i} is expressed in the following form owing to it having nothing to do with the initial conditions of the system:

$$q_{2i}(t) = \frac{1}{M_i \omega_{\mathrm{id}}} \int_0^t F(\tau) e^{-\xi_i \omega_i (t-\tau)} \sin \omega_{\mathrm{id}} (t-\tau) \mathrm{d}\tau_i. \tag{35}$$

The displacement of the system is expressed as follows:

$$\mathbf{y} = \mathbf{y}^0 + \mathbf{y}^*. \tag{36}$$

Here, $\mathbf{y}^0 = \sum_{i=1}^n \boldsymbol{\varphi}_i q_{1i}$ and $\mathbf{y}^* = \sum_{i=1}^n \boldsymbol{\varphi}_i q_{2i}$.

The displacement of the system can be represented as follows:

$$\mathbf{y}^* = \mathbf{y} - \mathbf{y}^0. \tag{37}$$

The following expressions can be obtained by introducing equations (33) and (35) into equation (37):

$$\mathbf{y}^* = \int_0^t \sum_{i=1}^n \frac{\boldsymbol{\varphi}_i \boldsymbol{\varphi}_i^T}{\mathbf{M}_i \omega_{\mathrm{id}}} \mathbf{S}_i(\tau) e^{-\xi_i \omega_i (t-\tau)} \sin \omega_{\mathrm{id}} z(t-\tau) \mathrm{d}\tau. \tag{38}$$

Usually, $\mathbf{y}^*(t)$ can be described as

$$\mathbf{y}^*(t) = \int_0^t \mathbf{G}(t-\tau) \mathbf{F}(\tau) \mathrm{d}\tau. \tag{39}$$

Hence, $\mathbf{G}(t)$ can be described by comparing equations (38) and (39):

$$G(t) = \sum_{i=1}^n \frac{\boldsymbol{\varphi}_i \boldsymbol{\varphi}_i^T}{\mathbf{M}_i \omega_{\mathrm{id}}} e^{-\xi_i \omega_i t} \sin \omega_{\mathrm{id}} t. \tag{40}$$

Let $\{\mathbf{y}^*(t)\} = \{y_1^*(t) \Lambda y_m^*(t)\}^T$, $\{\mathbf{F}(t)\} = \{F_1(t) \Lambda F_m(t)\}^T$, and $\{\mathbf{G}(t)\} = \{g_1(t) \Lambda g_m(t)\}^T$; then, equation (39) was discretized, and it is transformed into a matrix form that can be expressed as follows:

$$\begin{Bmatrix} y_1^* \\ y_2^* \\ y_3^* \\ \mathbf{M} \\ y_m^* \end{Bmatrix} = \begin{bmatrix} g_1 & 0 & 0 & \Lambda & 0 \\ g_2 & g_1 & 0 & \Lambda & 0 \\ g_3 & g_2 & g_1 & \Lambda & 0 \\ \mathbf{M} & \mathbf{M} & \mathbf{M} & \Lambda & 0 \\ g_m & g_{m-1} & g_{m-2} & \Lambda & 0 \end{bmatrix} \begin{Bmatrix} F_1 \\ F_2 \\ F_3 \\ \mathbf{M} \\ F_m \end{Bmatrix}. \tag{41}$$

or simply noted as

$$\mathbf{Y} = \mathbf{GF}. \tag{42}$$

Equation (42) can be expressed by the following form due to the responses containing noise:

$$\mathbf{Y}^c = \mathbf{GF}_{\mathrm{id}} + e. \tag{43}$$

Here, $\mathbf{F}_{id}$ is the identified dynamic force, e is the unknown noise, and $e = l \cdot \mathrm{std}(y(t)) \cdot \mathrm{rand}$. l is a parameter level, $\mathrm{std}(\cdot)$ is the standard deviation, and rand is a random number which ranges from −1 to 1.

Equation (43) is ill-conditioned, whose solution is usually astaticism. Then, it can be transformed into an optimization problem by using the Tikhonov regularization method [40]:

$$J(\mathbf{F}_{\mathrm{id}}) = \min \left\| \mathbf{GF}_{\mathrm{id}} - \mathbf{Y}^c \right\|^2 + \lambda \left\| \mathbf{F}_{\mathrm{id}} \right\|. \tag{44}$$

Equation (44) is considered as a kind of unconstrained optimization problem and a series of optimization algorithms, which can treat such unconstrained optimization problem. In our work, an efficient mixed spectral conjugate gradient (EMSCG) method was proposed to minimize equation (44).

4.2. Experimental Setup. In our work, a diagram of experimental setup is organized in Figure 2. The size of the coal-seam structure specimen manufactured artificially was 2000 mm × 800 mm × 1750 mm; the pick is mounted on the rotary cutting arm, and it can be driven by the reducer and torque; its power driven by the motor is rated at 55 kW. The cutting bench achieves free forward and backward movement by the hydraulic pressure drive control system. System output responses can be measured by the corresponding sensors, then converted by a signal amplifier, and finally recorded by a V10Dasp data vibration signal acquisition system [41].

The cutting force generated between pick and coal-seam structure is transmitted through the gear sleeve and measured by the force sensor at the back end. The measuring direction of the sensor and the cutting axis is defined as the axial load F_z. The measuring direction of the vertical the cutting axis is defined as the radial load F_y. The force

1-Motor;
2-Reducer;
3-Torque meter;
4-Slipping ring;
5-Cutting and force measuring device;
6-Coal-seam

Figure 2: A diagram of the experimental setup.

diagram of pick is shown in Figure 3. Z denotes the cutting force, Y denotes the propulsion resistance, f denotes the friction force between the supporting structure and the pick sleeve, β is the tangential installation angle of the pick, O is the supporting point of the gear sleeve, l_1 is the distance from the pick tip to the supporting point, and l_2 is the distance from the sensor to the supporting point. It is clearly seen from Figure 3 that the balance equation of force and the equilibrium equation of moment can be obtained, which is shown in the following equation:

$$\begin{cases} Y\cos\beta + Z\sin\beta - f = F_z, \\ (Y\sin\beta - Z\cos\beta)\cdot l_1 + F_y l_2 = 0, \\ l_1 f = (l_1 + l_2) f_n F_y. \end{cases} \tag{45}$$

By simplifying equation (45), the relationship between the cutting force Z and the axial load F_z, the radial load F_y and installation angle β are obtained, as shown in the following equation:

$$Z = F_z\sin\beta + F_y\left(f_n\sin\beta(1+k_l) + k_l\cos\beta\right), \tag{46}$$

where f_n is the friction coefficient between the gear sleeve and the supporting structure and $f_n = 0.1$ and k_l is the size coefficient of pick and sensor and $k_l = 0.739$.

In this experimental, the installation angle of conical pick is 45°, the maximum cutting thickness of the pick is 20 mm, the hauling speed is 0.8 r/min, and the rotary arm speed is 41 m/min. The measured axial load and radial load of the pick are shown in Figures 4(a) and 4(b), and the cutting force is converted by equation (15) according to the load curves shown in Figures 4(a) and 4(b), which is shown in Figure 4(c).

Under the above experimental conditions, it can be seen that although the value of cutting force is different from the axial load, the change trend is similar and the radial load has little effect on the change rule; that is, the cutting force Z is proportional to the axial load F_z. Therefore, the measured axial load can reflect the magnitude and variation of cutting force and can be approximately characterized by the measured axial load when analyzing the characteristics of cutting force.

4.3. Result Analysis. In order to study the influence of the proposed method on load identification results, and to compare with other methods, the results and methods are given. All codes were written in MATLAB 7.0 and run on a HP with 2.0 GB RAM and Windows 7 operating system. Stop the iteration if criterion is defined as $|g_k| \le 10^{-5}$ is satisfied or run time is more than 500 seconds. And the step length α_k is calculated by equation (3), the parameters are obtained as follows: $c = 0.1$ and $t = 1$.

For performance analysis of dynamic force identification methods used, the performance measurement metrics for dynamic force are described as follows: restoration time, iterative steps, and root mean-square-error (RMSE), where RMSE is defined by

$$\text{RMSE} = \sqrt{\frac{1}{N}\sum_{i=1}^{N}\left[Z_{\text{id}} - Z_{\text{actual}}\right]^2}, \tag{47}$$

where Z_{actual} is the actual force and Z_{id} is the identified force.

In order to effectively identify dynamic force generated between conical pick and coal-seam structure, first we provide the measured displacement response within 0.3 seconds which can be obtained by the finite element method, which is shown in Figure 5.

Since the measured displacement response can be given by the computed numerical solution, then we can use the present method in the paper to identify dynamic force based on the mathematical model of dynamic force identification [19, 20].

The identified results of dynamic force are achieved by using the different methods in this paper, which are shown in Figures 6(a)–6(d), respectively.

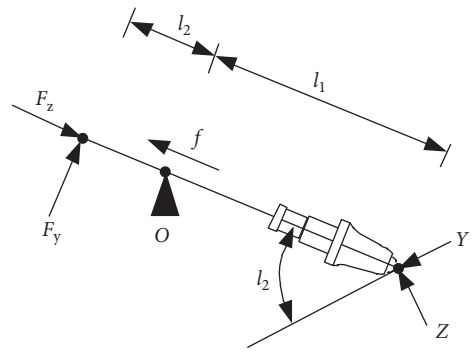

Figure 3: The force diagram of pick.

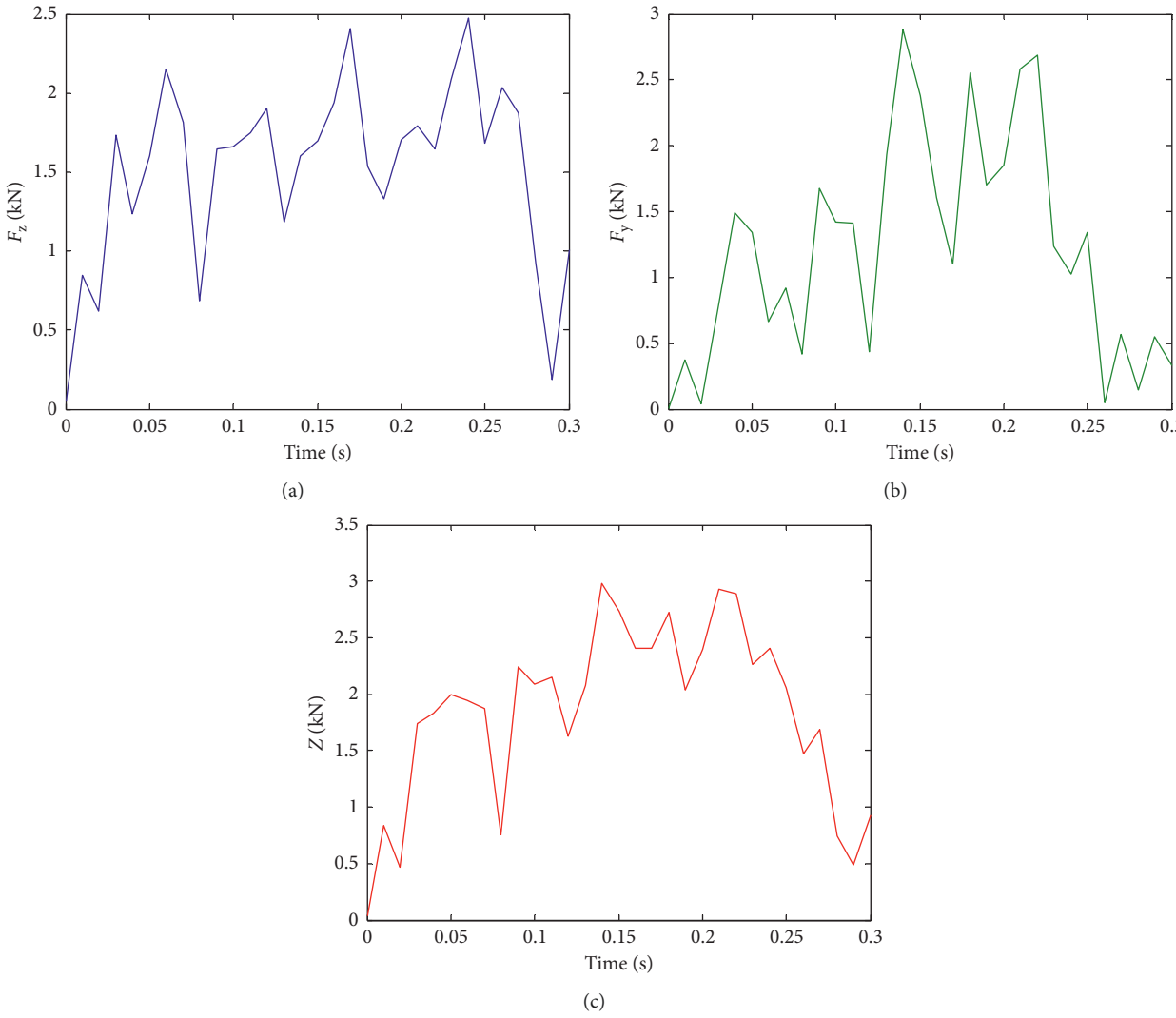

Figure 4: Cutting load and cutting force. (a) Axial load. (b) Radial load. (c) Cutting force.

We can see from Figures 6(a)–6(d) that the different methods can identify the dynamic force generated between conical pick and coal-seam structure from the measured displacement response by the finite element method. However, the performance of dynamic force identification results has a certain difference.

We can draw a conclusion from Table 1 that the present method makes it more successful to identify dynamic force

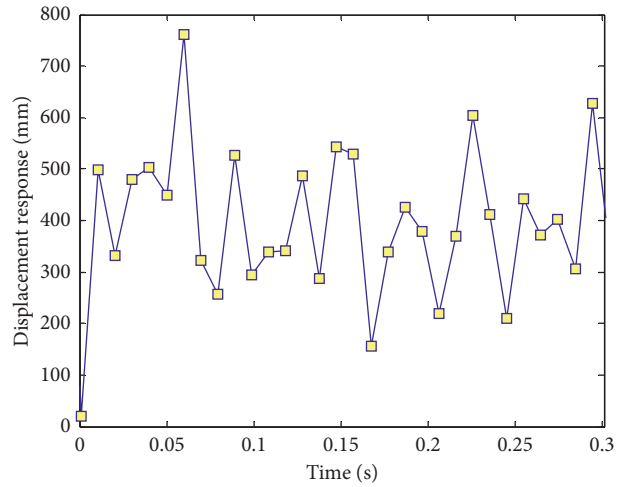

Figure 5: Measured displacement response.

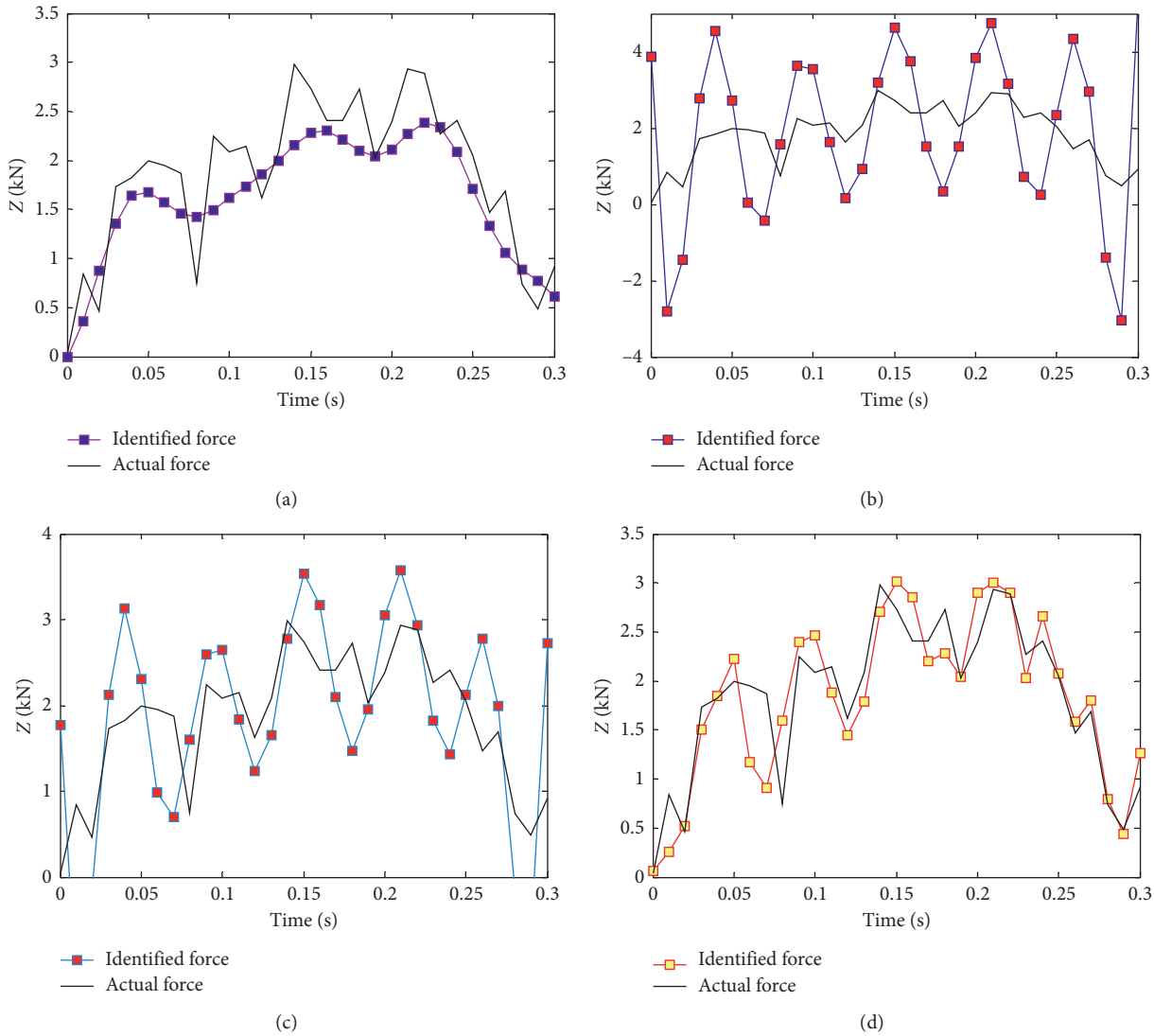

Figure 6: Identified results under different methods. (a) FR method. (b) PRP method. (c) VPRP method. (d) EMSCG method.

Table 1: Comparison of different identification methods.

Evaluation metrics	FR method	PRP method	VPRP method	EMSCG method
RMSE	0.4182	2.9087	0.9055	0.3665
Restoration time (s)	12.1442	40.3227	18.361	5.0116
Iterative steps	19	55	27	11

generated between conical pick and coal-seam structure based on the measured displacement response.

5. Conclusions

In this paper, an efficient mixed spectral conjugate gradient (EMSCG) method is proposed for the dynamic force identification. Moreover, the convergence of the proposed method based on the convergence analysis in Section 3 is strictly proved. An engineering example is investigated in Section 4, in which the performance of the proposed method is also compared with that of the existing methods. The analysis results show that the present method has high efficiency and very robust convergence performance and reduces the number of iterations. In addition, the proposed method can provide more efficient and numerically stable approximation of the actual force, compared with the FR method, PRP method, and VPRP method. The results validate the stability and the effectiveness of the present method, and there is reason to believe that the present method can offer a reference for future research.

Data Availability

No data were used to support this study.

Conflicts of Interest

The authors declare that they have no conflicts of interest.

Acknowledgments

This work was supported by the Chinese National Natural Science Foundation (Contract nos. 51674106 and 51274091).

References

[1] T. S. Jang, H. Baek, S. L. Han, and T. Kinoshita, "Indirect measurement of the impulsive load to a nonlinear system from dynamic responses: inverse problem formulation," *Mechanical Systems and Signal Processing*, vol. 24, no. 6, pp. 1665–1681, 2010.

[2] S.-J. Kim and S.-K. Lee, "Experimental identification for inverse problem of a mechanical system with a non-minimum phase based on singular value decomposition," *Journal of Mechanical Science and Technology*, vol. 22, no. 8, pp. 1504–1509, 2008.

[3] T. S. Jang, H. G. Sung, S. L. Han, and S. H. Kwon, "Inverse determination of the loading source of the infinite beam on elastic foundation," *Journal of Mechanical Science and Technology*, vol. 22, no. 12, pp. 2350–2356, 2008.

[4] Y. Dai, L. Liu, and S. Feng, "On the identification of coupled pitch and heave motions using opposition-based particle swarm optimization," *Mathematical Problems in Engineering*, vol. 2014, Article ID 784049, 10 pages, 2014.

[5] B. Blaschke, A. Neubauer, and O. Scherzer, "On convergence rates for the Iteratively regularized Gauss-Newton method," *Ima Journal of Numerical Analysis*, vol. 17, no. 3, pp. 421–436, 2018.

[6] J. Gao, D. Wang, and J. Peng, "A tikhonov-type regularization method for identifying the unknown source in the modified helmholtz equation," *Mathematical Problems in Engineering*, vol. 2012, Article ID 878109, 13 pages, 2012.

[7] C.-S. Liu, W. Qu, and Y. Zhang, "Numerically solving twofold ill-posed inverse problems of heat equation by the adjoint Trefftz method," *Numerical Heat Transfer, Part B: Fundamentals*, vol. 73, no. 1, pp. 48–61, 2018.

[8] J. N. Franklin, "Minimum principles for ill-posed problems," *SIAM Journal on Mathematical Analysis*, vol. 9, no. 4, pp. 638–650, 2012.

[9] L. Zhang, W. Yang, C. Shen, and J. Feng, "Error bounds of Lanczos approach for trust-region subproblem," *Frontiers of Mathematics in China*, vol. 13, no. 2, pp. 459–481, 2018.

[10] F. Stout and J. H. Kalivas, "Tikhonov regularization in standardized and general form for multivariate calibration with application towards removing unwanted spectral artifacts," *Journal of Chemometrics*, vol. 20, no. 1-2, pp. 22-23, 2006.

[11] A. Y. AL-Bayati and R. S. Muhammad, "New scaled sufficient descent conjugate gradient algorithm for solving unconstraint optimization problems," *Journal of Computer Science*, vol. 6, no. 5, pp. 1953–1958, 2010.

[12] W. W. Hager and H. Zhang, "The limited memory conjugate gradient method," *SIAM Journal on Optimization*, vol. 23, no. 4, pp. 2150–2168, 2013.

[13] Y. J. Wang, C. Y. Wang, and N. H. Xiu, "A family of supermemory gradient projection methods for constrained optimization," *Optimization*, vol. 51, no. 6, pp. 889–905, 2002.

[14] K. W. Ng and A. Rohanin, "Solving optimal control problem of monodomain model using hybrid conjugate gradient methods," *Mathematical Problems in Engineering*, vol. 2012, Article ID 734070, 14 pages, 2012.

[15] Y. Narushima and H. Yabe, "Global convergence of a memory gradient method for unconstrained optimization," *Computational Optimization and Applications*, vol. 35, no. 3, pp. 325–346, 2006.

[16] J.-B. Jian, Y.-F. Zeng, and C.-M. Tang, "A generalized supermemory gradient projection method of strongly sub-feasible directions with strong convergence for nonlinear inequality constrained optimization," *Computers & Mathematics with Applications*, vol. 54, no. 4, pp. 507–524, 2007.

[17] E. G. Birgin and J. M. Martinez, "A spectral conjugate gradient method for unconstrained optimization," *Applied Mathematics and Optimization*, vol. 43, no. 2, pp. 117–128, 2001.

[18] A. Y. Al-Bayati and H. N. Al-Khayat, "A global convergent spectral conjugate gradient method," *Australian Journal of Basic & Applied Sciences*, vol. 7, no. 7, pp. 302–309, 2013.

[19] C. Y. Wang and M. X. Li, "Convergence property of the Fletcher-Reeves conjugate gradient method with errors," *Journal of Industrial & Management Optimization*, vol. 1, no. 2, pp. 193–200, 2017.

[20] Z.-J. Shi and J. Shen, "Convergence of the Polak–Ribiére–Polyak conjugate gradient method," *Nonlinear Analysis: Theory, Methods & Applications*, vol. 66, no. 6, pp. 1428–1441, 2007.

[21] A. Qu, M. Li, Y. Xiao, and J. Liu, "A modified Polak–Ribiére–Polyak descent method for unconstrained optimization," *Optimization Methods and Software*, vol. 29, no. 1, pp. 177–188, 2014.

[22] Y. Nakatsukasa, T. Soma, and A. Uschmajew, "Finding a low-rank basis in a matrix subspace," *Mathematical Programming*, vol. 162, no. 1-2, pp. 325–361, 2017.

[23] B. Lu, Y. Cao, M. J. Yuan, and J. Zhou, "Reference variable methods of solving min-max optimization problems," *Journal of Global Optimization*, vol. 42, no. 1, pp. 1–21, 2008.

[24] N. Andrei, "Numerical comparison of conjugate gradient algorithms for unconstrained optimization," *Studies in Informatics and Control*, vol. 16, no. 4, pp. 333–352, 2007.

[25] X. Dong, D. Han, Z. Dai, L. Li, and J. Zhu, "An accelerated three-term conjugate gradient method with sufficient descent condition and conjugacy condition," *Journal of Optimization Theory and Applications*, vol. 179, no. 3, pp. 944–961, 2018.

[26] M. Rahmati, B. Huang, L. M. Schofield et al., "Effects of Ag promotion and preparation method on cobalt Fischer-Tropsch catalysts supported on silica-modified alumina," *Journal of Catalysis*, vol. 362, pp. 118–128, 2018.

[27] A. Vadakkepatt, S. R. Mathur, and J. Y. Murthy, "Efficient automatic discrete adjoint sensitivity computation for topology optimization–heat conduction applications," *International Journal of Numerical Methods for Heat & Fluid Flow*, vol. 28, no. 2, pp. 439–471, 2018.

[28] W. Zhou and X. Chen, "On the convergence of a derivative-free HS type method for symmetric nonlinear equations," *Advanced Modeling and Optimization*, vol. 3, pp. 645–654, 2012.

[29] X.-Z. Jiang and J.-B. Jian, "A sufficient descent Dai-Yuan type nonlinear conjugate gradient method for unconstrained optimization problems," *Nonlinear Dynamics*, vol. 72, no. 1-2, pp. 101–112, 2013.

[30] L. Y. Liu and Y. Li, "Global convergence of a conjugate gradient method with strong Wolfe-Powell line search," *Journal of Shandong University*, vol. 43, no. 56, pp. 54–56, 2008.

[31] J. K. Liu and Y. Y. Jiang, "Global convergence of a spectral conjugate gradient method for unconstrained optimization," *Abstract and Applied Analysis*, vol. 2012, Article ID 758287, 12 pages, 2012.

[32] Q. Chen and X. Z. Jiang, "A spectral conjugate gradient method for unconstrained optimization," *Journal of Yulin Normal University*, vol. 43, no. 2, pp. 117–128, 2016.

[33] A. G. Lu, H. W. Liu, X. Zheng, and W. Cong, "A variant spectral-type FR conjugate gradient method and its global convergence," *Applied Mathematics and Computation*, vol. 217, no. 12, pp. 5547–5552, 2011.

[34] K. R. Wang, W. Cao, and Y. H. Wang, "A spectral CD conjugate gradient method with Armijo-type line search," *Journal of Shandong University*, vol. 45, no. 11, pp. 104–108, 2010.

[35] X. Du and J. Liu, "Global convergence of A spectral Hs conjugate gradient method," *Procedia Engineering*, vol. 15, no. 5-6, pp. 1487–1492, 2011.

[36] L. Grippo and S. Lucidi, "Convergence conditions, line search algorithms and trust region implementations for the Polak–Ribière conjugate gradient method," *Optimization Methods and Software*, vol. 20, no. 1, pp. 71–98, 2005.

[37] J. K. Liu, X. L. Du, and K. R. Wang, "A mixed spectral CD-DY conjugate gradient method," *Journal and Applied Mathematics*, vol. 2012, Article ID 569795, 10 pages, 2012.

[38] J. C. Gilbert and J. Nocedal, "Global convergence properties of conjugate gradient methods for optimization," *SIAM Journal on Optimization*, vol. 2, no. 1, pp. 21–42, 1992.

[39] J. Liu, X. Sun, X. Han, C. Jiang, and D. Yu, "Dynamic load identification for stochastic structures based on Gegenbauer polynomial approximation and regularization method," *Mechanical Systems and Signal Processing*, vol. 56-57, pp. 35–54, 2015.

[40] C. S. Liu, C. P. Ren, and D. G. Li, "Reconstruction and deduction of cutting coal and rock load spectrum on modified discrete regularization algorithm," *Journal of China Coal Society*, vol. 39, no. 5, pp. 981–986, 2014.

[41] C. S. Liu, C. P. Ren, and F. Han, "Study on time-frequency spectrum characteristic of dynamic cutting load based on wavelet regularization," *Applied Mechanics and Materials*, vol. 577, pp. 196–200, 2014.